Barium titanate nanoparticles: Short-range lattice distortions with long-range cubic order

Chenyang Shi, Simon J. L. Billinge, Eric Puma, Sun Hwi Bang, Nathaniel J. H. Bean, Jean-Claude de Sugny, Robert G. Gambee, Richard C. Haskell, Adrian Hightower, and Todd C. Monson

Phys. Rev. B **98**, 085421 — Published 15 August 2018

DOI: 10.1103/PhysRevB.98.085421

Barium titanate nanoparticles: short-range lattice distortions with long-range cubic order

Chenyang Shi[1] and Simon J. L. Billinge[1,2]

Eric Puma[3], Sun Hwi Bang[4], Nathaniel J. H. Bean[5], Jean-Claude de Sugny[4], Robert G. Gambee[4], Richard C. Haskell[5], Adrian Hightower[4], and Todd C. Monson[6]*

[1] Department of Applied Physics and Applied Mathematics, Columbia University, New York, New York 10027, USA

[2] Condensed Matter Physics and Materials Science Department, Brookhaven National Laboratory, Upton, New York 11973, USA

[3] Physics Department, Pomona College, Claremont, California 91711, USA

[4] Engineering and [5] Physics Departments, Harvey Mudd College, Claremont, California 91711, USA

[6] Nanoscale Sciences Department, Sandia National Laboratories, Albuquerque, New Mexico 87185, USA

ABSTRACT: Barium titanate (BTO) nanoparticles (sizes 10 to 500 nm) exhibit a displacement of the Ti atom from the center of the Perovskite unit cell as inferred from synchrotron X-ray diffraction patterns (XRD) analyzed using atomic pair distribution functions (PDFs). Fits to PDFs acquired at temperatures of 20° to 220°C indicate that these Ti displacements (~ 0.1 Å) are comparable to or even greater than those in the bulk material. Moreover, these displacements persist at temperatures well above 120°C where the tetragonal to pseudo-cubic phase transition occurs in the bulk. Tetragonal Raman spectral lines were observed for all sizes of these BTO nanoparticles and confirm a distorted unit cell up to 120°C. Above 120°C, the small BTO nanoparticles (10, 50, 100 nm) continue to display tetragonal Raman lines, though with slowly decreasing amplitudes as the temperature rises. In contrast, the tetragonal Raman lines of large BTO nanoparticles (300, 400, 500 nm) disappear abruptly above 120°C, suggestive of bulk material. Indeed, fits to large-particle X-ray PDFs over the range 20-60 Å reveal a sharp, long-range structural change toward a cubic lattice at 120°C, again consistent with bulk material. This sharp, long-range structural change is absent in the small particles. In fact, laboratory XRD Bragg peak profiles for the small BTO particles appear to be singlets at 20°C, indicating that significant long-range cubic order already exists at room temperature. As temperature rises, this long-range cubic order is gradually reinforced as inferred from long-range fits of the small particle PDFs. By combining information from X-ray PDFs, Raman spectra, and Bragg peak profiles, we conclude that small BTO nanoparticles exhibit both short-range (unit-cell) distortion and long-range (mesoscale) cubic order from 20° to 220°C, while the large nanoparticles behave as bulk material, differing from small particles only by exhibiting long-range tetragonal order below 120°C and a mesoscale structural phase change at 120°C.

I. INTRODUCTION

The effective use of renewable energy, smart grids, and electric vehicles is critically dependent upon the next generation of electrostatic capacitors and their promise for increased energy storage and enhanced power conversion and conditioning. Fine-grained ceramic capacitors (using 5 to 50 nm particles) can offer benefits which include higher breakdown strength, improved electromechanical performance, and reduced permittivity dependence on field and temperature.[1-3] Barium titanate ($BaTiO_3$ or BTO) has long been a favorite dielectric material for electrostatic capacitors; it is ferroelectric at room temperature with an effective dielectric constant of 1500-2000.[4] However, there is still some debate as to whether the ferroelectric properties of BTO will persist or perhaps even strengthen in nanoparticle form.

In bulk form, BTO assumes four crystallographic phases.[5] Below -90°C (183 K), the ground state crystal structure is rhombohedral ($R3m$); it is ferroelectric with Ti displacements aligned along a body diagonal <111>. Between -90° and 5°C, BTO is orthorhombic ($Amm2$) and is again ferroelectric but with net polarization along a face diagonal <011>. Between 5° and 120°C, it is tetragonal ($P4mm$) and remains ferroelectric with polarization now along the z-axis <001>. Above 120°C, BTO becomes paraelectric, exhibits long-range cubic order, and is generally assigned a cubic ($Pm\bar{3}m$) crystal structure.

Two models were proposed in the 1960s to describe these phase transitions and associated changes in direction of polarization. In the displacive model proposed by Cochran[6], "soft" phonon modes drive the phase transitions and result in Ti displacements along the <111>, <011>, and <001> directions in the rhombohedral, orthorhombic, and tetragonal phases, respectively, and predict a centered Ti ion in the cubic phase. In the 8-site order-disorder model proposed by Bersuker[7] and Comes et al.,[8,9] each Ti ion is displaced along one of eight

<111> directions in all four phases, but with the eight possible positions populated differently in different phases. In the rhombohedral phase, the Ti ions occupy the same position in all unit cells, yielding a polarization along <111>. In the orthorhombic phase, two adjacent body-diagonal positions are occupied with equal probability yielding polarization along <011>, while for the tetragonal phase, four positions are populated equally resulting in polarization along <001>. In the cubic phase, all eight positions are equally populated, leading to zero net polarization and an average position of the Ti ion at the center of the cubic unit cell. Clearly, the 8-site order-disorder model predicts the same *average* structure as the displacive model, but predicts a different *local* structure leading to diffuse X-ray scattering which was first observed by Comes et al.[8,9] Since then, Kwei et al.[10] have measured neutron total scattering from BTO just above and below the rhombohedral-to-orthorhombic transition. Using PDF analysis, they confirmed the difference between local (short-range) structure and crystallographic (long-range or average) structure as predicted by the 8-site order-disorder model. More recently Page et al.[11] performed neutron PDF analysis and found Ti displacements along <111> in their room temperature bulk BTO sample, a departure from the expected tetragonal lattice and in support of the Comes model.

Within the past few years, Levin et al.[12] and Senn et al.[13] have independently used neutron PDF analysis and complementary techniques to show collectively and convincingly that Ti off-centering displacements in bulk BTO are directed approximately along <111> for all three ferroelectric phases as well as for the highest-temperature paraelectric phase. Thus the differences between local and average structure predicted by the 8-site order-disorder model have been observed in bulk BTO in all three higher temperature phases. Finally, we note that these observations of differences between local and average structure are in agreement with the XAFS/XANES studies reported by Ravel et al.[14] for bulk BTO.

BTO nanoparticles: Small BTO nanoparticles (≤ 100 nm) exhibit many but not all properties possessed by the pseudo-cubic phase of bulk BTO above 120°C. The critical question for applications in energy storage is whether BTO nanoparticles can be made to exhibit ferroelectricity or whether the observed Ti displacements will necessarily be averaged spatially (and/or temporally) to zero by random or ordered arrangements of small groups of polarized unit cells. To address this question, we have studied the structure of BTO nanoparticles ranging in size from 10 to 500 nm using three techniques sensitive to short and/or long range order: (1) synchrotron X-ray pair distribution function (PDF) analysis (short or long range), (2) Raman scattering (short and long range for our wavenumbers and back-scattering geometry), and (3) examination of laboratory XRD Bragg (200) reflections (long range).

Our results in this paper are arranged as follows: Section II describes the sample preparation and measurement techniques employed for structural characterization. In Section III we present PDFs calculated from synchrotron 2-D XRD patterns acquired at temperatures ranging from room temperature (RT) to 493 K (220°C). Fits to these PDFs reveal significant Ti displacements (~ 0.1 Å) for all sizes of particles and at all temperatures, including above 120°C where bulk BTO is in the pseudo-cubic phase. Previous researchers have used X-ray or neutron PDF analyses to observe similar Ti displacements in BTO nanoparticles at room temperature.[11,15-17] Here we extend these published PDF results to temperatures above RT and well beyond 120°C.

Section IV contains Raman spectra for BTO nanoparticles ranging in size from 10 to 500 nm and for temperatures ranging from RT to 493 K (220°C). These Raman studies confirm the unit cell distortions observed with X-ray PDF on the same nanoparticle samples, and also agree with a previous temperature study of Raman spectra for BTO nanoparticles.[16]

Section V is devoted to laboratory XRD scans of Bragg (200) peaks at room temperature for all seven sizes (10 to 500 nm) of BTO nanoparticles examined in our labs. These peak profiles document the transition from tetragonal doublets (due to lattice distortions) to apparent cubic singlets indicating long-range cubic order as the particle size decreases from 500 to 10 nm.

In Section VI, Summary and Discussion, we combine results from all three experimental techniques to paint a consistent picture of the behavior of the BTO nanoparticles examined in these studies. For example, we conclude that the 500 nm particles are sufficiently large to serve as a good proxy for bulk BTO. These large particles exhibit a dramatic long-range (mesoscale) structural change as the temperature rises through 120°C that leaves them with the well-known long-range cubic order characteristic of the bulk phase of BTO at elevated temperatures.

For the small BTO nanoparticles (≤ 100 nm) at RT, our three types of experimental data indicate significant Ti displacements (~ 0.1 Å) but only slight distortions of the crystal lattice when measured over a large spatial scale. These small lattice distortions yield the familiar Bragg (200) singlets indicative of long-range cubic order. Similar observations were previously reported by Smith et al.[16]

At 120°C and above, these small BTO nanoparticles continue to exhibit significant Ti displacements yet progressively smaller lattice distortions when measured over a large spatial scale. Unlike the larger 500 nm BTO particles, the small BTO nanoparticles show no dramatic long-range structural change at 120°C, but rather reinforce slowly their long-range cubic order with rising temperature. Again, the small lattice distortions yield the familiar Bragg (200) singlets indicative of long-range cubic order.[16]

A full understanding of the structural coherence of these small BTO nanoparticles is essential for their successful application in high-density energy storage. While we have woven together a consistent picture of their short-range structure from measurements of Ti displacement and unit cell distortion, we cannot yet discern the precise arrangement of polarized unit cells that yields long-range cubic order.

II. MATERIALS & METHODS

A. BTO nanoparticle samples

Two different sources of BTO nanoparticles were used in these studies. First, BTO nanoparticles were obtained commercially from Sakai Chemical Industry Co., Ltd. (Japan) in a series of sizes: 50 nm (KZM-50), 100 nm (BT-01), 200 nm (BT-02), 300 nm (BT-03), 400 nm (BT-04), and 500 nm (BT-05). According to the manufacturer, an improved hydrothermal process was used to synthesize these particles.[18] For ease of discussion in this report, we have renamed these particles BT50, BT100, BT200, BT300, BT400, and BT500, where the numerals indicate the size in nm.

Second, 10 nm BTO particles were synthesized at Sandia National Laboratories (SNL) using an alkoxide-hydroxide synthesis first developed and reported by Yoon, Baik, and coworkers[19] and modified to obtain more precise control over water addition and achieve better particle dispersion. We have labeled these particles BT10. The BT10 particles were synthesized through the hydrolysis of barium hydroxide octahydrate ($Ba(OH)_2 \cdot 8H_2O$, 98+%, Acros, New Jersey, USA) and titanium isopropoxide ($Ti[OCH(CH_3)_2]_4$, 98+%, Acros), followed by the condensation of excess water. The reaction was performed in a fume hood using air-free chemistry techniques which included the use of a Schlenk line that allowed the reaction flasks to remain closed to the environment and under flowing nitrogen gas. All glassware was rinsed with ethanol and maintained in a drying oven until just prior to the synthesis. The barium hydroxide octahydrate (0.1 mol) and titanium isopropoxide (0.1 mol) were added to ethanol (20 mol; C_2H_6O, 100%, Pharmco-Aaper, Brookfield, Connecticut, USA) at room temperature under vigorous stirring. The ethanol was dried over molecular sieves for 24 hr. and sparged with nitrogen overnight. The solution was then heated to 80ºC in a water bath, and deionized water (6 mol, sparged overnight with nitrogen) was added slowly to the solution in a dropwise fashion using a peristaltic pump. After all the water was added, the solution was allowed to reflux for 60 min. The solution was then centrifuged at 4500 rpm for 10 min. and washed, first with deionized water and then ethanol. If used in powder form, the particles were dried in a vacuum oven at 60°C overnight.

B. Synchrotron X-ray PDF analysis

Synchrotron X-ray total scattering experiments were conducted on beamline X17A at the National Synchrotron Light Source (NSLS) at Brookhaven National Laboratory. The samples were packed into kapton capillary tubes, and high energy X-ray diffraction measurements were performed at room temperature (RT) through 493 K (220°C) with a step-size of 10 K using a cryostream. The rapid acquisition pair distribution function (RaPDF) technique[20] was used with an X-ray energy of 67.42 keV (λ = 0.1839 Å). A large area 2-D Perkin Elmer detector (2084 × 2084 pixels and 200 × 200 μm pixel size) was mounted orthogonal to the beam path with a sample-to-detector distance of ~204 mm. The raw 2D data were azimuthally integrated and converted to 1D intensity versus 2θ using FIT2D.[21] PDFgetX3[22] was used to correct and normalize the diffraction data and then Fourier transform them to obtain the PDF, $G(r)$, according to $G(r) = {}^{2}/_{\pi} \int_{Q_{min}}^{Q_{max}} Q[S(Q)-1] sinQr\, dQ$. Here Q is the magnitude of the momentum transfer on scattering, and $S(Q)$ is the properly corrected and normalized powder diffraction intensity measured from Q_{min} to Q_{max}.[23] A value for Q_{max} of 25 Å^{-1} was used for all particle sizes except BT10, in which case a value of 20 Å^{-1} was used. $G(r)$ gives the probability of finding a pair of atoms separated by a distance r. Lanthanum hexaboride (LaB_6) served as the standard material for BT500 and BT50 to calibrate the sample-to-detector distance and to determine Q_{damp} and Q_{broad}, which are the parameters that correct the PDF envelope function for instrument resolution effects.[24,25] The refined values are Q_{damp} = 0.03828 Å^{-1} and Q_{broad} = 0.01790 Å^{-1}. The standard material for BT200, BT100, and BT10 was nickel (Ni), and the associated values for Q_{damp} and Q_{broad} are 0.03956 Å^{-1} and 0.01749 Å^{-1}, respectively. The values for Q_{damp} and Q_{broad} are allowed to vary in subsequent model fits to PDF data.

The PDF modelling was carried out using the PDFgui program.[25] For each sample we tried two possible space groups/structural models for $BaTiO_3$:[5,17,26] (1) $Pm\bar{3}m$ (No. 221) (cubic) where Ba, Ti and O atoms are on (0, 0, 0), (1/2, 1/2, 1/2) and (0, 1/2, 1/2), respectively, and (2) $P4mm$ (No. 99) (tetragonal) where Ba, Ti, O1 and O2 are on (0, 0, 0), (1/2, 1/2, z), (1/2, 1/2, 0) and (0, 1/2, 1/2), respectively. Note that in the tetragonal model the displacement of the Ti atom is constrained to the z-direction. See Fig. 1. More will be said about this constraint in Section III. The lattice constant a is a fitting parameter in both cubic and tetragonal models, and the lattice constant c is an additional fitting parameter in the tetragonal model. Isotropic atomic displacement parameters U_{iso} are assigned to Ba, Ti, and O (just one for both Wykoff positions) as fitting parameters in both models.

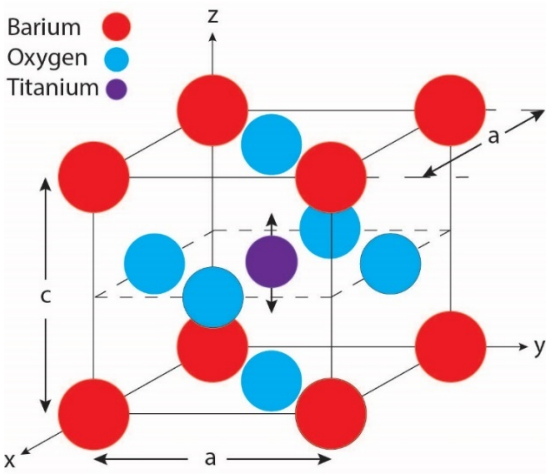

FIG. 1. The tetragonal lattice model is shown with its lattice parameters a and c and the possible displacement of Ti along the z-axis.

C. Raman spectra

Samples of BTO nanoparticles were placed in a 4 mL cylindrical glass vial (15 mm diam. × 45 mm high). The vial was placed in an aluminum block (49.2 mm × 49.2 mm × 55.6 mm high) with a 15.9 mm hole drilled to accept the vial and a 6.35 mm hole to allow the passage of the incident laser beam. The 532 nm laser beam (90 mW) from a Lambda Solutions, Inc., Dimension P-1 Raman System (LSI, Waltham, Massachusetts USA) was coupled via optical fiber through an LSI Microscope Raman Adaptor and focused with a Nikon LU Plan Fluor microscope objective (10x, 0.30 NA, 17.5 mm WD, $^{\infty}/_{0}$) through the glass vial and into the BTO sample. Backscattered light was collected by the incident optics, passed through a spectrometer, and relayed ultimately to the CCD detector array which was cooled to -70°C.

Raman spectra were acquired at room temperature before and after a temperature scan that typically began at 220°C and ended at 60°C. The BTO nanoparticle sample in the glass vial and aluminum block were heated in an oven to 220°C and then transferred to the Raman setup and allowed to cool while spectra were acquired. A type K thermocouple (Control Company #4003, Friendswood, Texas USA) was inserted into a small hole in the side of the aluminum block and provided

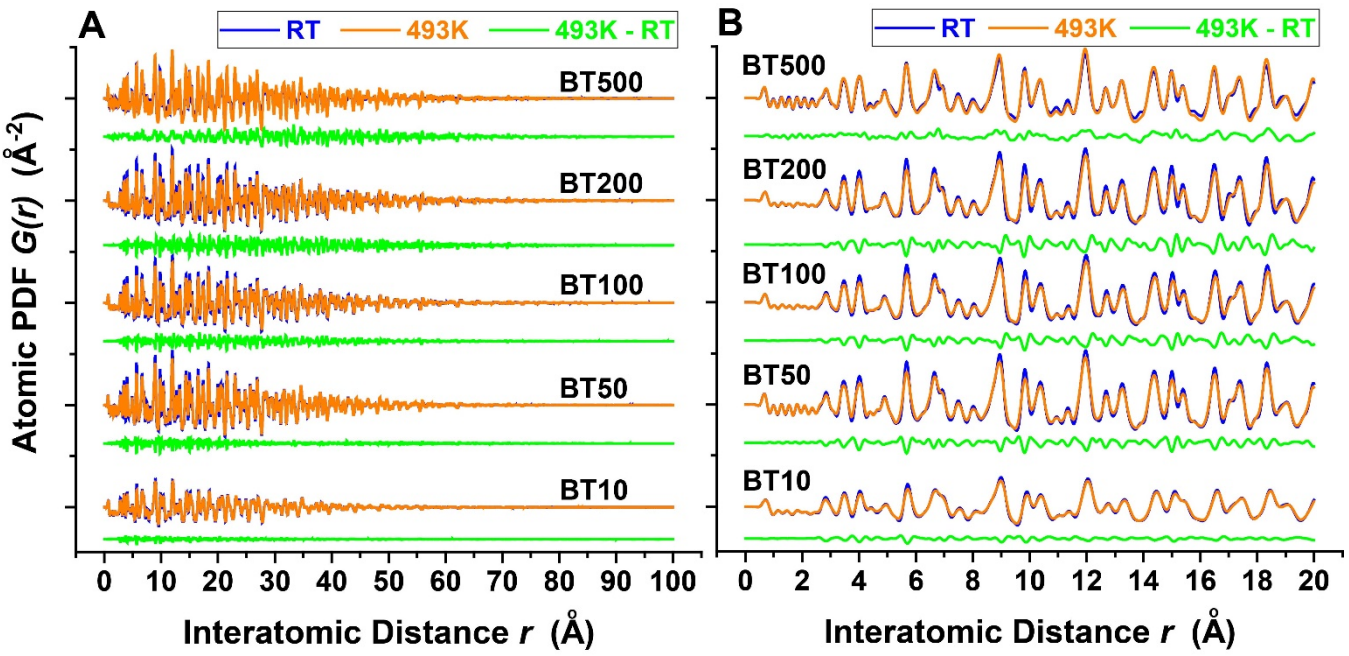

FIG. 2. Pair distribution functions (PDFs) at room temperature (RT) (blue) and 493K (220°C) (orange) are superposed. Differences (green) are displaced for clarity. Panel A displays the PDFs over a 100 Å range, while panel B zooms in to a 20 Å range and provides a glimpse of the small but visible changes over the full range of temperatures explored.

the temperature of the block, vial, and BTO sample. Initial cooling from 220°C proceeded at a rate of 7°C/min and slowed to 1°C/min at 60°C. Acquisition of a Raman spectrum required 5 sec.

D. Laboratory XRD – Bragg (200) peaks

A Rigaku Ultima IV X-ray Diffractometer was used to acquire XRD Bragg reflections of BTO nanoparticle samples. The instrument was operated at 40 kV and 44 mA and employed a copper target. Scans of the BTO Bragg (200) peak were performed in 0.01° increments of 2θ at a speed of 0.05°/min. For calibration purposes, similar scans were performed of the Bragg (220) peak of silicon powder (325 mesh, 44 μm particle size, Sigma Aldrich) between scans of BTO nanoparticles. All measurements were performed at room temperature.

III. SYNCHROTRON PDF ANALYSIS

Pair distribution functions (PDFs) were calculated from XRD data acquired at temperatures ranging from room temperature (RT) to 493 K (220°C). Figure 2 displays the superposition of PDFs at RT and 493 K for each of the five BTO particle sizes that were examined. Panel A plots the PDFs to an interatomic distance r = 100 Å. Note that only the 10 nm particle PDFs exhibit a shortened decay length indicative of a limited structural coherence length. Other PDFs decay approximately as their respective standard materials (see Section II), indicating that over the range plotted their decay lengths cannot be distinguished from bulk material.

Figure 2B provides a zoomed-in view of the same PDFs plotted to r = 20 Å and allows closer examination of the small changes between the PDFs at the extreme ends of the temperature range. Figure 3 is similar to Fig. 2B but superposes PDFs at 373 K (100°C) and 423 K (150°C), temperatures that are just below and above the tetragonal to pseudo-cubic transition at 120°C in BTO bulk material.[5] Very little of the differences displayed in Fig. 2B seem to occur around 120°C. Hence it is

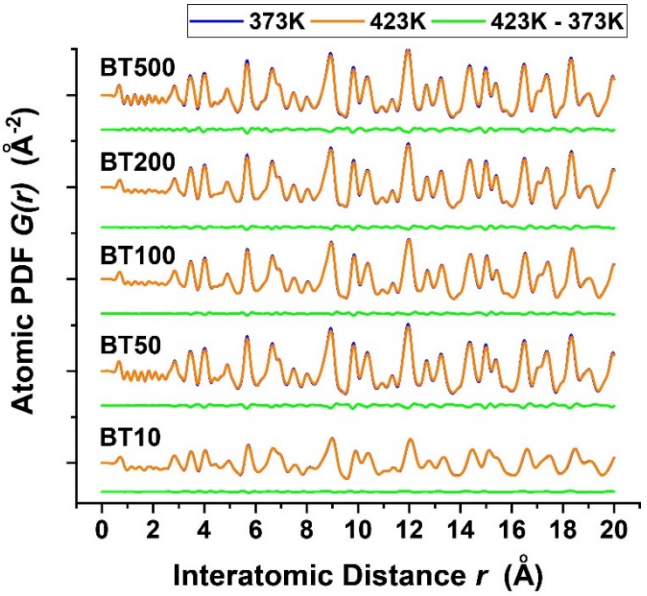

FIG. 3. PDFs at 373 K (100°C) (blue) and 423 K (150°C) (orange) are superposed. Differences (green) are displaced for clarity. Note that the differences are much smaller than in Fig. 2B; little of the change in Fig. 2B occurs around 120°C.

not visually obvious that any of the BTO nanoparticles undergo the phase transition observed in bulk BTO which would be expected to perturb the PDFs across the phase transition.

To search for phase transitions and to obtain robust and reliable values for structural parameters, we found it necessary to fit PDFs over a significant range of r, e.g., 1 to 20 Å or 20 to 60 Å. Fits over the range 1 to 20 Å should provide a good picture of short-range structure, while fits over 20 to 60 Å should be more sensitive to the long-range cubic structure observed in the pseudo-cubic phase above 120°C in bulk

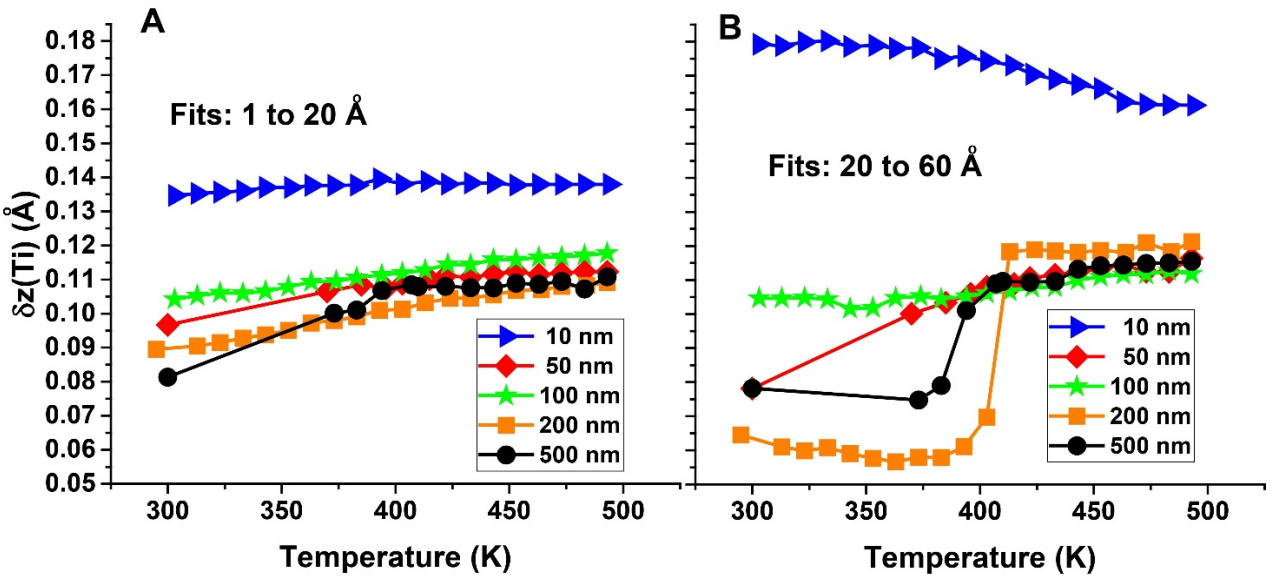

FIG. 4. The z-displacement of the Ti atom (in Å) is plotted as a function of temperature. (**A**) The data plotted has been derived from fits to PDFs over the range r = 1 to 20 Å and should provide a good picture of the short-range structure of the lattice. (**B**) The data has been derived from fits to PDFs over the range r = 20 to 60 Å and should reflect the longer-range structure of the lattice. The 200 & 500 nm BTO nanoparticles exhibit a long-range structural phase change around 120°C (390 K).

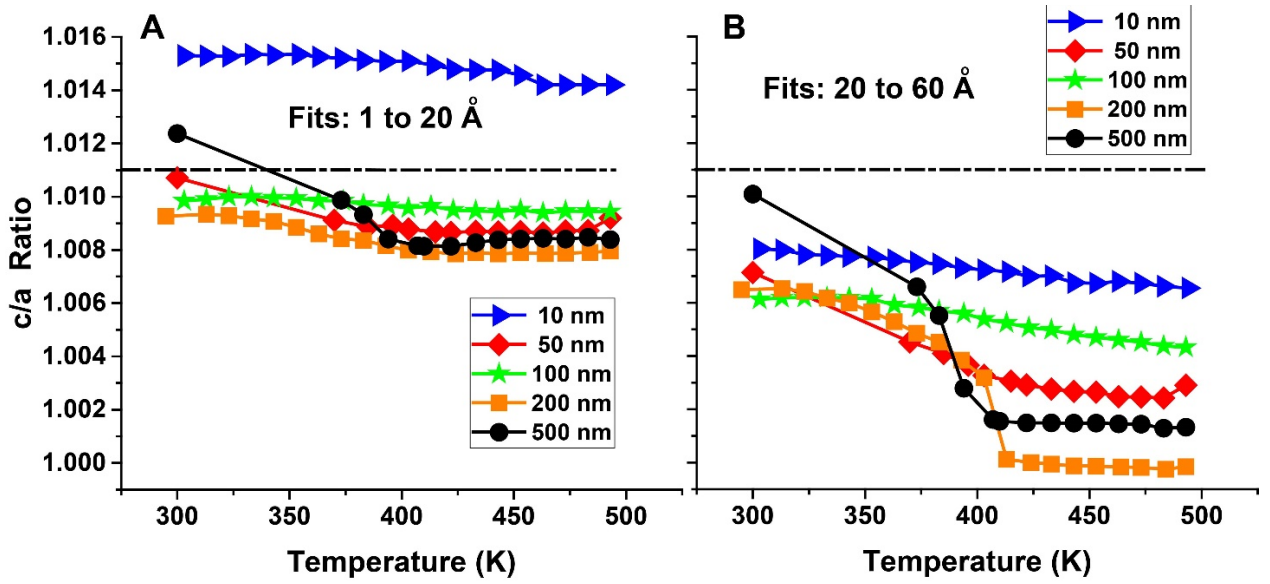

FIG. 5. The c/a ratio of the lattice is plotted as a function of temperature. (**A**) The data plotted has been derived from fits to PDFs over the range r = 1 to 20 Å and should provide a good picture of the short-range structure of the lattice. (**B**) The data has been derived from fits to PDFs over the range r = 20 to 60 Å and should reflect the longer-range structure of the lattice. Note that this longer-range perspective yields substantially reduced distortions (c/a values) than are plotted in panel A. Also note that the largest particles (200 & 500 nm) show a structural phase change around 120°C (390 K) when viewed from a longer-range perspective. The dash-dot line indicates the c/a ratio (1.011) exhibited by bulk BTO at RT.[5]

BTO. We used two model lattices for these fits: (1) a cubic model with the Ti atom fixed at the center of the Perovskite unit cell, and (2) a tetragonal model with the Ti atom allowed to displace from the center along the z-axis. (For more details see Section II and Fig. 1.) For comparison, we also used a tetragonal model with Ti displacements along a body diagonal. See Section III.D.

Section S.III and Fig. S.1 of the Supplemental Material[32] display measured PDFs for 500 nm BTO particles with fits using both cubic and tetragonal models at temperatures just below and above 120°C and over short and long ranges of the interatomic distance *r*. The plots of the data with fits illustrate the importance of fitting over significant ranges of *r* to extract precise and robust values for structural parameters.

A. Off-centering of Ti in the unit cell

Figure 4 plots the fitted *z*-displacements of the Ti atom from the center of the unit cell as a function of temperature for all five particle sizes examined. Panel A displays the values resulting from fits over a 1 to 20 Å *r*-range, while B reports the results for a 20 to 60 Å range. The short-range Ti displacements in Panel A generally increase with increasing temperature. Fits over the long *r*-range in Panel B exhibit a sharp

increase in displacement around 120°C (393 K) for the 200 & 500 nm BTO particles. We interpret this behavior in the large nanoparticles to be suggestive of the phase transition observed in bulk BTO. The curves of the smaller sizes of nanoparticles do not indicate they experience a phase transition.

Figure 5 displays the fitted values of the c/a ratio, i.e., the "tetragonality" of the lattice, as a function of temperature for all five particle sizes examined. Again, Panel A reports the results of fits to a 1 to 20 Å *r*-range, and B shows values from the 20 to 60 Å range. Note that the long-range values plotted in Panel B are significantly lower than those in Panel A, indicating a trend toward a long-range cubic order. Also in Panel B, the c/a ratios for the 200 & 500 nm particles exhibit sharp decreases in tetragonality around 120°C (393 K), possibly indicating a phase change toward long-range cubic order. The curves for the 10, 50, and 100 nm particles do not show evidence of this phase change. We shall see that the Raman data presented in Section IV and the Bragg peak profiles presented in Section V provide strong support for the conclusion that the 500 nm BTO particles serve as a viable proxy for bulk BTO, while the 200 nm particles are slightly too small to behave entirely as bulk.

Fitted values for the individual lattice parameters *a* and *c* are plotted in Fig. S.2 in the Supplemental Material[32] as a function of temperature. The PDF fits were performed over the *r*-range of 1 to 20 Å for the data plotted in Fig. S.2.

B. Structural coherence of the nanoparticles

All results presented in Figs. 4 and 5 are derived from fits to PDFs using the tetragonal lattice model and two *r*-ranges for the fits: 1 to 20 Å and 20 to 60 Å. Using the larger *r*-values (20 to 60 Å) probes the sample on a larger spatial scale and should give insight into the extent of the structural coherence of the nanoparticles. Figure 6 displays the fitted results for the Ti *z*-displacement and the ratio *c/a* using progressively larger *r*-ranges: 1 to 20 Å, 1 to 30 Å, 1 to 40 Å, 1 to 50 Å, and 1 to 60 Å. Room temperature PDFs for all five particle sizes were used to generate this figure. Panel A in Fig. 6 shows the Ti displacement increasing slightly with increasing *r*-range, then leveling off at an *r*-range of about 40 Å. Rabuffetti and Brutchey[17] report a similar result for the Ti *z*-displacement dependence on *r*-range (see their Fig. 9(d)). Smith et al.[16] report a similar dependence on *r*-range for the distortion parameter *D* (see their Fig. 10) which they define to be:
$D \equiv [(\text{Ba-Ti})_{long} - (\text{Ba-Ti})_{short}] / [(\text{Ba-Ti})_{long} + (\text{Ba-Ti})_{short}]$.

Panel B of Fig. 6 shows the ratio *c/a* decreasing with increasing *r*-range for all particle sizes. Rabuffetti and Brutchey[17] report a similar trend for *c/a* with increasing *r*-range (see their Fig. 9(c)). The reduction of the refined *c/a* ratio with increasing *r* comes about presumably because of averaging over tetragonal domains with different orientations, returning toward a metrically cubic structure when enough domains of different orientation are sampled. This crossover behavior seems to be complete by around 40 Å which places the average size of the tetragonally distorted domains somewhat less than this.

It is noteworthy that the limited structural coherence invoked to explain the decrease in *c/a* in Fig. 6B does not seem to influence the Ti displacement in Fig. 6A in a similar way. These results have been described as "counterintuitive"[17] and "not completely understood".[16] The present authors cannot provide a conclusive and compelling explanation.

C. Tetragonal versus cubic lattice models

Figure 6B demonstrates that fitting PDFs over *r*-ranges that include large *r*-values probes the sample on a larger spatial scale and begins to reveal a trend toward long-range cubic order. Several BTO nanoparticle sizes exhibit long-range cubic order in certain temperature ranges. For example, as described in Section V, the laboratory XRD Bragg peaks of small BTO particles (≤ 100 nm) display small *c/a* ratios and hence long-range cubic order at room temperature. Moreover, Smith et al.[16] report cubic order at 148°C for 70 nm BTO particles. Similarly, the Bragg peaks of large BTO particles (≥ 300 nm, effectively bulk) suggest long-range cubic order above 393 K (120°C).[16] It would seem reasonable then to expect a cubic lattice model to perform comparably to a tetragonal model when fitting X-ray PDFs over the range r = 20 to 60 Å for these cases of expected long-range cubic order. We tested this expectation by comparing cubic vs. tetragonal fits of PDFs for all particle sizes at RT and 493 K (220°C).

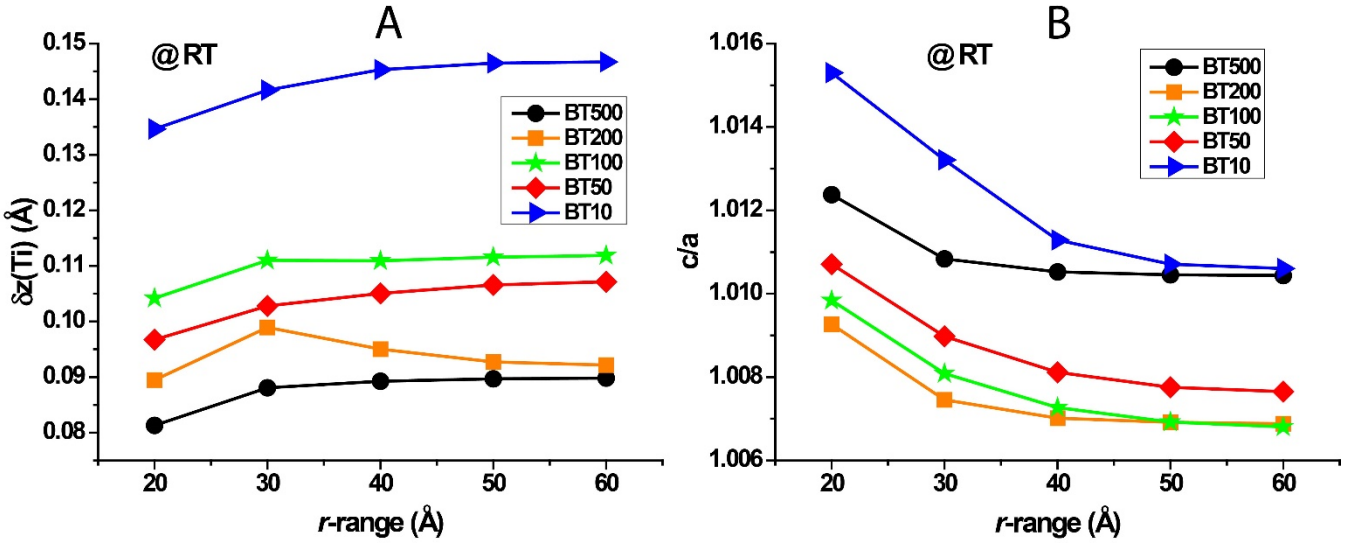

FIG. 6. The Ti *z*-displacement and *c/a* ratio at room temperature are plotted versus the *r*-range over which the PDFs are fitted. All five particle sizes show a slight increase in Ti displacement with increasing range, while the c/a ratio decreases substantially. The trends in Figs. 4 & 5 are consistent with the more detailed, stepwise trends in the present figure.

Figure 7 plots the cubic-to-tetragonal ratios for the residual function R_w[27] as a function of particle size. Also plotted are the associated cub/tet ratios of the fitted values for the isotropic atomic displacement factors U_{iso} for titanium, barium, and oxygen.

Using the residual function R_w as the criterion, long-range cubic fits to the X-ray PDFs (r = 20 to 60 Å) are indeed comparable to those of the tetragonal lattice in those cases when long-range cubic order is expected. The large cub/tet ratio for R_w for the 500 nm particles in Fig. 7A is expected because lab XRD data indicate the long-range order of these particles is in fact tetragonal at RT. In general, the slightly larger cubic values for R_w displayed in Fig. 7 are expected because the cubic model has two fewer fitting parameters. However, the cubic fits generally suffer from unusually large cub/tet ratios for Ti U_{iso} compared to those for Ba and O (see Fig. 7B), evidently due to the persistent short-range off-centering of Ti which cannot be accommodated in a truly cubic model. For this reason, we have always fit with both tetragonal and cubic models even when the pseudo-cubic structure is expected.

D. Ti displacements along a body diagonal

In the results reported above we have followed the lead of previous researchers[11,15-17] who used a tetragonal model with Ti displacements constrained to the z-axis, as might seem natural in the displacive model.[6] However, Ti displacements along a body diagonal would seem more compatible with the 8-pt order-disorder model.[7-10,12,13] In Section S.III.D of the Supplemental Material,[32] we compare fits to BT100 PDFs at RT using both tetragonal lattice models. (See Fig. S.3.)

In Fig. S.3A we confirm for both models the trends for Ti displacement and *c/a* ratio exhibited in Fig. 6 (above). While there are hints emerging from our data analysis that suggest Ti off-centering may occur along a body diagonal rather than the z-axis, the case is not compelling.

IV. RAMAN SPECTRA vs. TEMPERATURE

Raman spectra were acquired from the full set of BTO nanoparticle powders over the same temperature range, RT to 220°C. Three prominent spectral lines were observed at 290, 510, and 710 cm^{-1} (see Figs. 8 & 9). Rabuffetti and Brutchey[17] recently surveyed the Raman literature and concluded that the 290 cm^{-1} spectral line is due to E(TO), E(LO), and B_1 phonons propagating in non-centrosymmetric tetragonal BTO. Similarly, they found that the 710 cm^{-1} line is associated with a tetragonal lattice and is assigned to A_1(LO) and E(LO) phonons. Indeed, in our larger BTO nanoparticles (300, 400, & 500 nm), we see the 290 and 710 cm^{-1} lines drop dramatically in amplitude as the temperature is raised above 120°C and the phase transitions from a tetragonal to a pseudo-cubic lattice (Figs. 8A & S.5). However, when the size of the particles is reduced to 200 nm or less, these tetragonal Raman lines continue above 120°C, albeit with slowly decreasing amplitude (Figs. 8B & 9).

The 510 cm^{-1} Raman line has long been observed in both tetragonal and cubic phases of BTO.[16,17,28] From their survey of the Raman literature, Rabuffetti and Brutchey conclude that the 510 cm^{-1} line is due to A_1(TO) phonons.[17] Because first-order Raman scattering is forbidden by symmetry for a perfect cubic lattice ($Pm\bar{3}m$ space group), the observation of A_1(TO) phonons in the pseudo-cubic phase of BTO implies that some sort of distortion occurs from a perfect cubic lattice. As discussed in Section III above, the Ti atom displacements from the center of the unit cell persist well above 120°C where the phase of the 500 nm BTO particles transitions to the pseudo-cubic lattice. In Fig. 8, note that the amplitude of the 510 cm^{-1} line decreases with increasing temperature, and the linewidth broadens, but the line clearly persists above 120°C. Several groups of researchers[16,17,28,29] have attributed the presence of the 510 cm^{-1} Raman line above 120°C to Ti displacements from the center of the TiO_6 octahedra. These could be random displacements, or they could be more ordered displacements as in the antiferroelectric (AFE) model of Zhang et al.[29] As the nanoparticles become smaller, the abrupt disappearance of the tetragonal 290 and 710 cm^{-1} lines above 120°C gives way

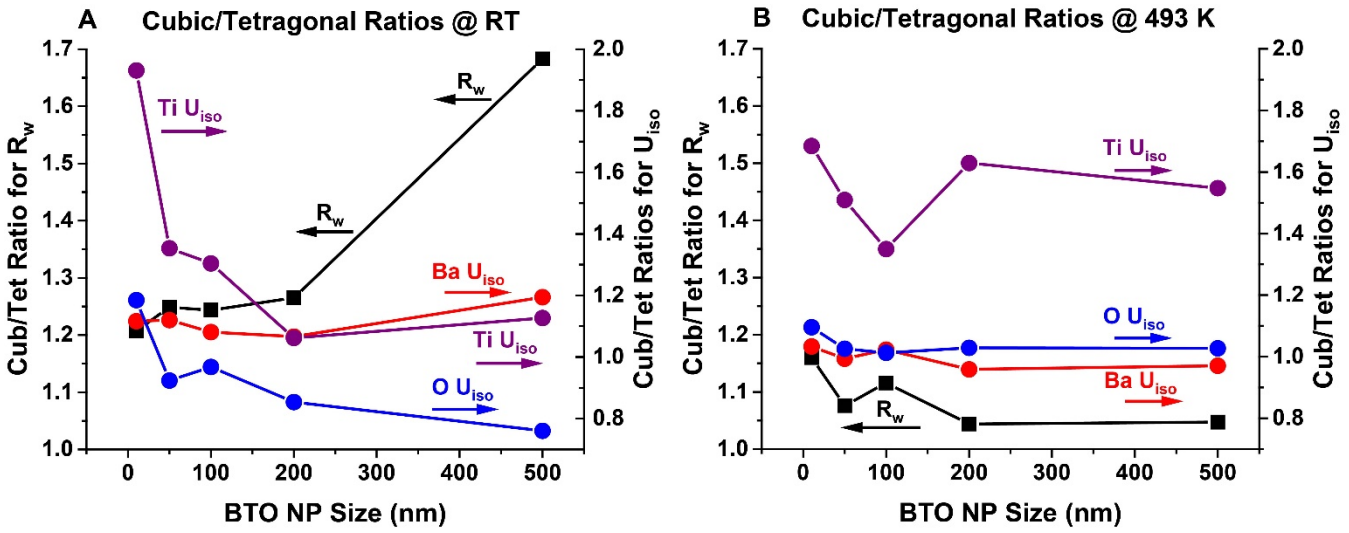

FIG. 7. Cubic/tetragonal ratios from fits to PDFs over r = 20 to 60 Å. Ratios for R_w and the U_{iso}'s for Ti, Ba, and O are plotted in Panel A as a function of BTO particle size for X-ray PDF data acquired at room temperature (RT). A similar plot appears in Panel B for data acquired at 493 K (220°C).

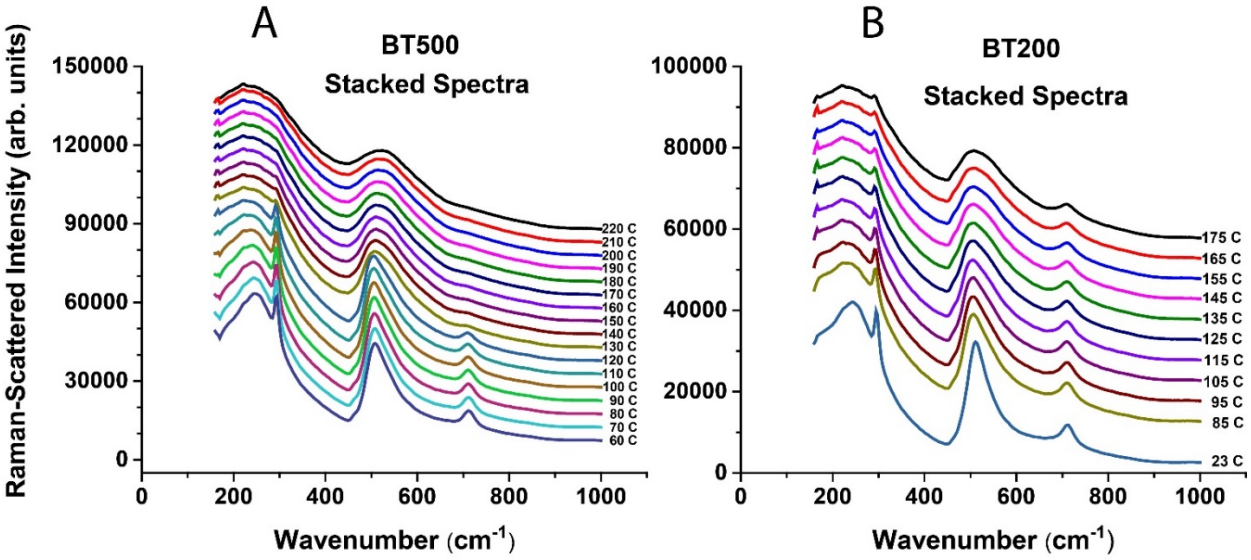

FIG. 8. Raman spectra versus temperature for (A) 500 nm and (B) 200 nm BTO particles. For BT500, the 290 and 710 cm^{-1} lines disappear abruptly above 120°C, while the 510 cm^{-1} line persists. For BT200, the amplitudes of the 290 and 710 cm^{-1} lines are reduced above 120°C, though definitely present.

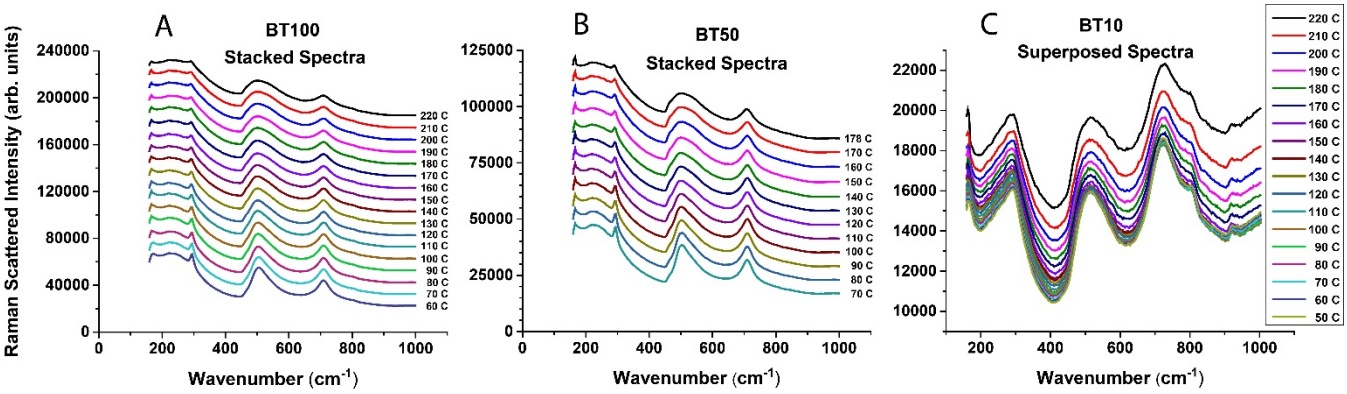

FIG. 9. Raman spectra versus temperature for (A) 100 nm and (B) 50 nm and (C) 10 nm BTO particles. Note that the 290 and 710 cm^{-1} tetragonal Raman lines persist even more strongly above 120°C as the particle size decreases. For the 10 nm particles, the Raman spectra are superposed (not stacked), and the lines are very broad and sit on top of a strong temperature-dependent background.

to a gradual reduction of the amplitudes of these lines with rising temperature. Figure 9 shows the behavior of 100, 50, and 10 nm BTO particles. The tetragonal 290 and 710 cm^{-1} lines are clearly present above 120°C, though their amplitudes are reduced. In the case of BT10, all three spectral lines are broad and persist above 120°C without noticeable attenuation.

A. Lorentzian fits to the tetragonal Raman lines

To quantify the temperature dependences of the amplitudes, widths, and frequencies of the tetragonal spectral lines at 290 and 710 cm^{-1}, Lorentzian profiles were fit to the lines at all temperatures and for four sizes of BTO particles: 500, 200, 50, and 10 nm. (Spectra for 100 nm particles are sufficiently similar to those of the 200 nm particles that we have omitted detailed analysis of the 100 nm particles.) In all cases presented here, a quadratic background was included in the Lorentzian fitting function to account partially for the increasing background in each spectrum with rising temperature. See Figs. S.6 & S.7 in Section S.IV in the Supplemental Material[32] for examples of fits to spectra of 500 nm and 50 nm particles.

Figure 10 presents the results of Lorentzian fits to the tetragonal 290 and 710 cm^{-1} lines at all temperatures for 500 nm BTO particles. Note that the amplitudes of the fitted Lorentzians decrease dramatically for the 290 and 710 cm^{-1} lines as the temperature rises through 120°C and the structure transitions from tetragonal to the pseudo-cubic lattice. At the same time, the widths of the lines increase somewhat more gently.

Figure 11 presents the same information for the 50 nm BTO particles. The reduction in amplitude of the lines as the temperature rises through 120°C is now a factor of ~3.5 less than that of the 500 nm particles, and the sharp drops of the curves in Fig. 10 are missing. The increases in the widths of the lines are a factor of ~2 less than for the 500 nm particles. There is no evidence of a phase transition at 120°C.

Similar plots for 200 nm and 10 nm BTO particles can be found in Section S.IV of the Supplemental Material.[32] Those plots, Figs. S.8 & S.9, show no evidence of a phase change at 120°C.

For all particle sizes, the frequencies of the tetragonal 290 and 710 cm^{-1} lines remain notably stable with temperature, varying in every case by less than 1.3%.

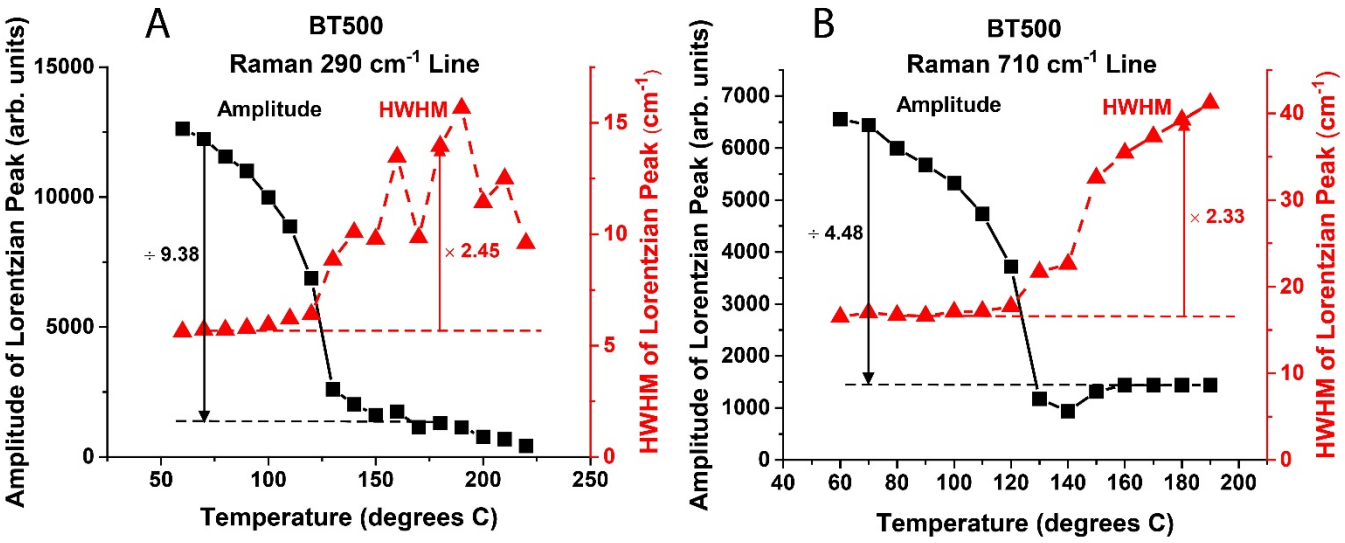

FIG. 10. The amplitude and half-width-at-half-maximum (HWHM) of a Lorentzian function fitted to the Raman 290 cm^{-1} line (A) and 710 cm^{-1} line (B) are plotted vs. temperature for 500 nm BTO particles. The fitted amplitudes decrease sharply while the width increases as the temperature rises through 120°C.

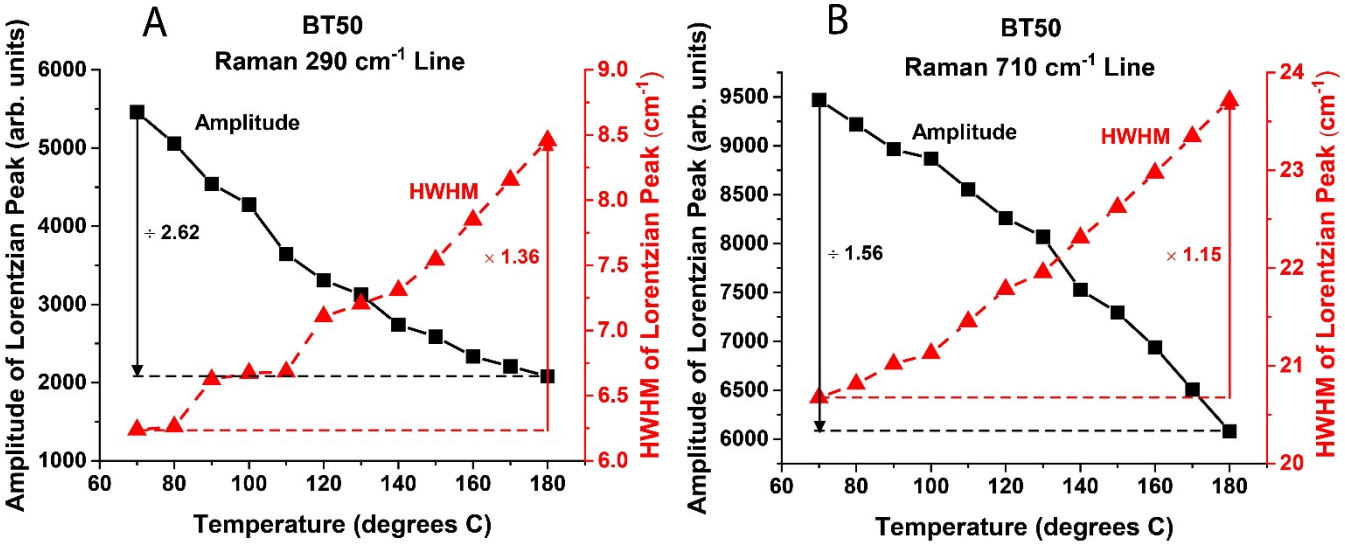

FIG. 11. The amplitude and HWHM of a Lorentzian function fitted to the Raman 290 cm^{-1} line (A) and 710 cm^{-1} line (B) are plotted vs. temperature for 50 nm BTO particles. The fitted amplitudes decrease steadily with no hint of the sharp drops of the curves in Fig. 10, while the width increases as the temperature rises through 120°C.

The temperature dependence of the tetragonal 290 and 710 cm^{-1} Raman spectral lines is summarized in Table 1 for four particle sizes. As the size of the BTO nanoparticle decreases, the reduction in amplitude decreases as the temperature rises above 120°C where, at least in bulk BTO material, the lattice transitions from tetragonal to the pseudo-cubic lattice. That is, with decreasing size nanoparticles, the tetragonal 290 and 710 cm^{-1} lines persist above 120°C with increasing strength. Indeed, as Fig. 11 illustrates, it is difficult to identify a phase transition as the 50 nm BTO particles rise through and well above 120°C.

It is important to note that the fitted amplitudes listed in Table 1 have been corrected [i.e., divided by n(ω)+1] for the Bose-Einstein thermal factor which predicts *increases* of 17% and 6% for the 290 and 710 cm^{-1} line amplitudes, respectively, over a temperature rise from 70° to 180°C, as opposed to the observed *decreases*.

Table 1. Temperature dependence of the Raman lines

BTO Sample	290 cm^{-1}		710 cm^{-1}	
	Amp[a]	HWHM[b]	Amp[a]	HWHM[b]
BT500	÷ 9.38	× 2.45	÷ 4.48	× 2.33
BT200	÷ 4.37	× 1.51	÷ 1.87	× 1.22
BT50	÷ 2.62	× 1.36	÷ 1.56	× 1.15
BT10	÷ 1.36	× 1.02	÷ 1.33	× 1.03

[a]A factor decrease in the Raman line amplitude as the temperature rises from 70° to 180°C is indicated by "÷ factor".

[b]A factor increase in the Raman line HWHM as the temperature rises from 70° to 180°C is indicated by "× factor".

V. LAB XRD BRAGG PEAKS

Bragg (200) peaks were recorded for the full set of Sakai BTO nanoparticles as well as the 10 nm particles synthesized at Sandia. All laboratory XRD scans were performed at room temperature. Figure 12 provides a stacked display of the (200) peaks for all particle sizes. The tetragonal double-peaked profile is evident for the 500, 400, and 300 nm particles, reflecting the two unequal lattice constants *a* and *c*. The peak on the right (larger 2θ) is due to the smaller lattice constant *a* [(200) and (020) peaks] and has twice the intensity of the peak on the left (smaller 2θ) [(002) peak] because of the two lateral dimensions spanned by *a*. Also note that both peaks comprising a tetragonal doublet are themselves doublets due to the K_α splitting of the instrument's Cu target. The tetragonal splitting is 0.51° in 2θ, while the Cu K_α splitting is about $1/4^{th}$ of that (0.12° in 2θ). Ordinarily the Cu K_α splitting is considered an instrumental nuisance, but in this case it provides a convenient measure of profile resolution.

The most striking feature of Fig. 12 is the transition from a clear tetragonal doublet for large sizes of BTO nanoparticles (500, 400, 300 nm) to an apparent cubic singlet Bragg peak for smaller sizes (100, 50, 10 nm). The 200 nm particles (BT200) seem to fall midway between the doublet and singlet ends of this transition.

Figure 13A provides a closer view of the (200) and (002) Bragg peaks for the larger BTO particles. While the BT500 (500 nm) and BT400 (400 nm) profiles are very similar, the BT300 (300 nm) is beginning to show fill-in between the (200) and (002) peaks. BT200 (200 nm) still shows some indication of a tetragonal splitting, but the magnitude of the splitting seems to be smaller, and the two peaks [(200) and (002)] are no longer well-resolved.

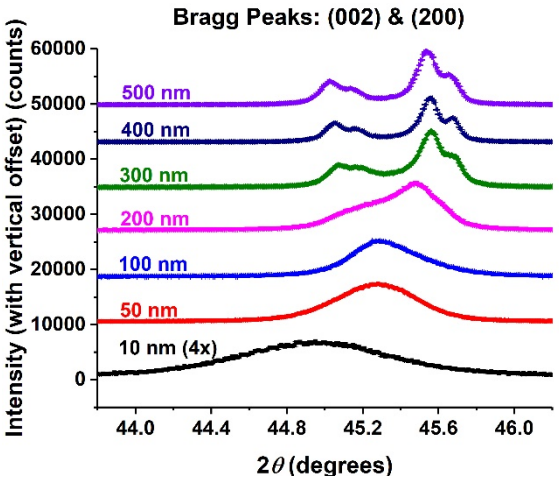

FIG. 12. Scans of the (200) and (002) Bragg reflection peaks are displayed for BTO nanoparticle sizes of 500, 400, 300, 200, 100, 50, and 10 nm. The 10 nm data are increased by 4x.

Figure 13B provides a closer view of the singlet Bragg (200) peaks scanned from BTO nanoparticle sizes of 10, 50, and 100 nm. The scan of the 200 nm particles is included to make connection with Fig. 13A and the larger nanoparticles with their tetragonal doublet Bragg peaks. The BT10 Bragg peak is clearly shifted to lower values of 2θ, indicating an expansion of the lattice at this smallest size (10 nm). There seems to be no remnant remaining in the profiles of BT10, BT50, and BT100 of the tetragonal splitting present in the larger sizes of BTO particles. These apparent singlet Bragg peaks suggest a long-range cubic structure.

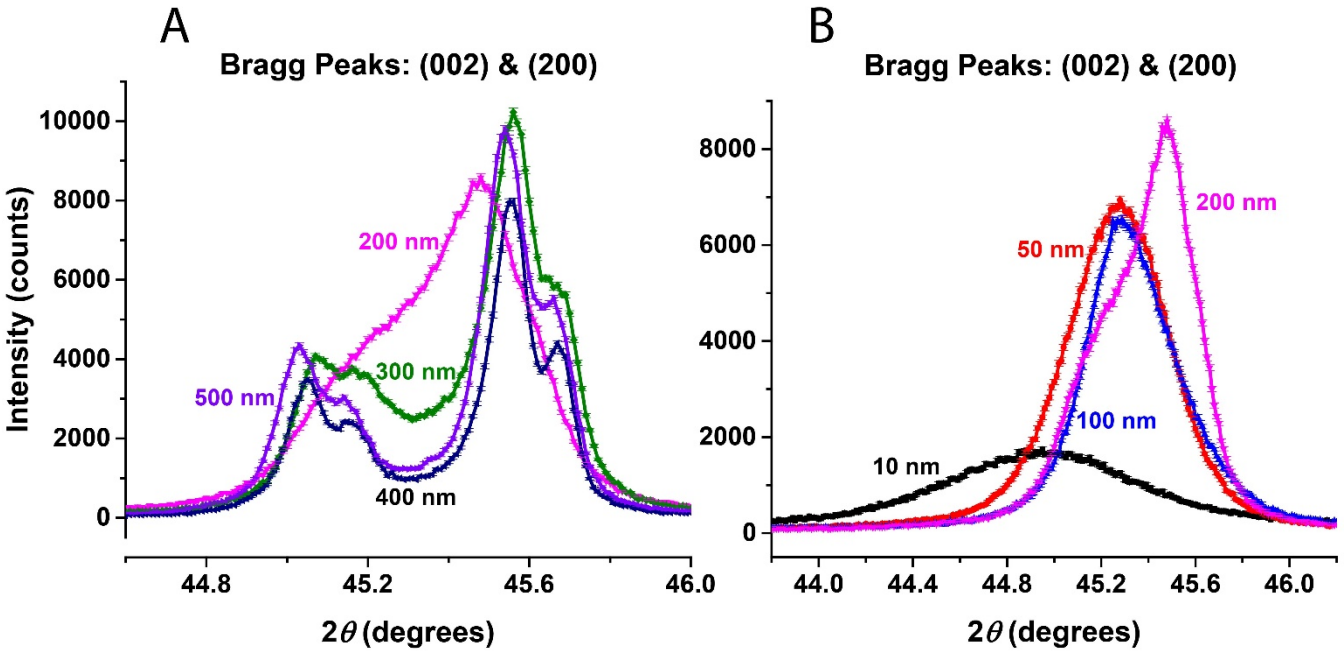

FIG. 13. Scans of the (200) and (002) Bragg peaks are displayed for BTO nanoparticle sizes of (A) 500 (violet), 400 (navy), 300 (olive), and 200 nm (magenta), and (B) of 10 (black), 50 (red), 100 (blue), and 200 nm (magenta). Note the tetragonal double peaks in (A) for the larger BTO nanoparticles – 500, 400, and 300 nm – and the cubic singlets in (B) for the smaller particles – 100, 50, and 10 nm.

A. Are the cubic singlets in fact tetragonal doublets?

Section S.V.A in the Supplemental Material[32] examines in more detail the apparent cubic singlet Bragg peaks in Fig. 13B. (See Fig. S.8.) Specifically, the BT100 Bragg peak profile in Fig. 13B is compared with several simulated profiles generated with values of the ratio *c/a* obtained from fits to PDFs at RT and plotted in Fig. 5B.

These comparisons suggest that the apparent cubic singlet Bragg peaks for the small BTO particles may in fact be tetragonal doublets but with reduced splittings that render them unresolvable under the width of the Bragg reflection profile.

VI. SUMMARY & DISCUSSION

Our synchrotron X-ray PDF analysis of BTO nanoparticles (Section III) concludes that the Ti atom is significantly displaced (~ 0.1 Å) from the center of the unit cell over the entire range of temperatures explored and for all particle sizes examined. We have used the fits to PDFs acquired at all temperatures to assemble a consistent but only partially complete picture of the structure of these nanoparticles over the range RT to 493 K (220°C). It has been essential to employ fits to the PDFs over the range r = 1 to 20 Å for best sensitivity to short-range structure and also over r = 20 to 60 Å to provide the long-range structure sensed by the Bragg (200) reflections. Figures 4 & 5 present the results of fits for both r-ranges for the Ti displacement and the ratio *c/a* for all temperatures and particle sizes examined.

A. Large BTO nanoparticles (≥ 300 nm) at RT

The fits to the PDFs for BT500 and especially the Raman spectra (Section IV) suggest that these large 500 nm BTO particles experience a phase transition similar to that of bulk BTO at 120°C. Indeed we regard BT500 as a proxy for bulk material. Figure 5B plots a PDF-fitted value for *c/a* of 1.0101(3) (r = 20 to 60 Å) at room temperature (RT), close to the literature value of 1.0110(2) for bulk derived from XRD patterns.[5] The value *c/a* = 1.0101 is also consistent with the observation of tetragonal Raman lines (290 and 710 cm^{-1}) (see Fig. 8A). Figure 4 reports a PDF-fitted value for the Ti displacement of about 0.08 Å (r = 20 to 60 Å) at RT, a significant displacement that certainly breaks cubic symmetry and allows the observation of the Raman 510 cm^{-1} line (see Fig. 8A). Finally, the lab XRD Bragg (200) reflection for BT500 is an easily resolved tetragonal doublet indicating a tetragonal lattice at room temperature (see Figs. 12 & 13A). The observed tetragonal splitting for BT500 in Figs. 12 & 13A is 0.51(1)° in 2θ which implies a value for *c/a* of 1.0107(4), in agreement with the literature value 1.0110(2) derived from XRD patterns for bulk BTO.[5]

B. Large BTO nanoparticles above 120°C

Let us now consider the structure of BT500 above 120°C in the presumed pseudo-cubic phase. Figure 4 reports the fitted Ti displacements for BT500 above 120°C. Values obtained from PDF-fits over both r = 1 to 20 Å and 20 to 60 Å hover around 0.11 Å, certainly sufficient to break the cubic symmetry and continue to allow the observation of the Raman 510 cm^{-1} line (see Fig. 8A). Moreover, Fig. 5 reports decreasing fitted values for *c/a* leading up to 120°C. Figure 5B shows a precipitous drop around 120°C that stabilizes at 1.0015, a value that would lead to a tetragonal Bragg peak doublet with a 2θ splitting of 0.07° which would be unresolvable under the Bragg profile, especially at temperatures over 120°C. (See Fig. S.7 in the Supplemental Material[32] for a relevant example involving BT100.) This result is consistent with a pseudo-cubic phase. Moreover, while there is no discontinuity in *c/a* at 120°C (see Fig. 5B), there is a dramatic drop in *c/a* and a discontinuity in slope (Fig. 5B) that signal some sort of structural transition that is consistent with the dramatic reduction in amplitudes of the tetragonal Raman lines (290 and 710 cm^{-1}) in Figs. 8A & 10. It is interesting to note that the BT200 curves in Figs. 4B & 5B show transitions at 120°C as sharp as the BT500 curves. However, the BT200 tetragonal Raman lines persist above 120°C, albeit with reduced amplitudes (see Fig. 8B). Moreover, the Bragg profiles in Figs. 12 & 13 indicate that 200 nm seems to be the particle size that divides those particles showing some long-range cubic order at RT from those that do not. In the face of this ambivalent behavior, we do not apply the "equivalent-to-bulk" label to BT200.

In support of our conclusion that the 500 nm BTO particles are sufficiently large to be regarded as bulk BTO, we note again that several groups of researchers[12-14] have reported significant Ti displacements in bulk BTO both below and above 120°C, just as we see in BT500. In addition, Arlt et al.[4] show in their Fig. 3 that 280 nm BTO particles exhibit a permittivity vs. temperature curve that is devoid of a phase transition at 120°C, while the curves for 700 nm and 6.8 μm particles display an obvious peak at the Curie temperature.

C. Small BTO nanoparticles (≤ 100 nm) at RT

BT10, BT50, and BT100 exhibit a somewhat different behavior. At room temperature, these small nanoparticles yield lab XRD Bragg reflections that seem to be cubic singlets, and most researchers describe the structure of these small nanoparticles as cubic or pseudo-cubic at RT. Indeed, many commercial manufacturers of these small BTO particles describe their structure as "crystallographically cubic".[30] On the other hand, Smith et al.[16] were able to detect a tetragonal broadening of the Bragg (400) reflection for a 70 nm BTO nanoparticle sample at room temperature. Upon raising the temperature to 148°C, they observed the broadening to decrease, leaving an apparent cubic singlet. In addition, in Section S.V.A of the Supplemental Material,[32] we analyze the RT Bragg (200) reflection of BT100 which seemed initially to be a cubic singlet. However, after recognizing that XRD, a long-range probe, will see a reduced value of *c/a* = 1.0061 (PDF fit over r = 20 to 60 Å), we realized the Bragg (200) profile could be concealing a tetragonal doublet with a reduced splitting.

Raman spectra provide another indication that the room temperature "pseudo-cubic" phase of small BTO nanoparticles is more nuanced than simply cubic. BT10, BT50, and BT100 exhibit tetragonal Raman lines (290 and 710 cm^{-1}) (see Fig. 9). The observation of these tetragonal Raman lines is consistent with *c/a* ratios of 1.008, 1.007, and 1.006, respectively, and Ti displacements of 0.10, 0.08, and 0.18 Å, respectively, deduced from PDF fits over r = 20 to 60 Å (see Figs. 4B & 5B). The Ti displacements also explain the observation of the 510 cm^{-1} Raman line which is forbidden in a perfectly centrosymmetric (cubic) lattice.

D. Small BTO nanoparticles above 120°C

The Ti displacements exhibited by BT10, BT50, and BT100 are slightly greater above 120°C than at room temperature (see Fig. 4). These substantial Ti displacements are consistent with the continued observation of the Raman 510 cm^{-1} line (see Fig. 9).

For BT10, BT50, and BT100, the values for *c/a* above 120°C can be seen in Fig. 5B to be smaller than at RT. Hence for

these small BTO particles, the long-range *c/a* values both below and above 120°C are small enough to cause the tetragonal splitting of a Bragg reflection to be concealed by the width of the peak. (See Section S.V.A of the Supplemental Material[32] for a full description of this phenomenon involving BT100.) Hence lab XRD Bragg reflections for these small BTO nanoparticles are usually interpreted as indicating a cubic (or pseudo-cubic) lattice structure at both RT and above 120°C.

On the other hand, the *c/a* values for these small particles (1.004 to 1.010, see Fig. 5B) are arguably large enough to be consistent with the observation of tetragonal Raman lines (290 and 710 cm^{-1}) from RT through well above 120°C. (See Fig. 9.) As mentioned above, the value of *c/a* does not seem to be a critical criterion by itself. BT500 with *c/a* = 1.003 above 120°C does not exhibit tetragonal Raman lines, but BT200 with *c/a* = 1.002 *does* exhibit tetragonal Raman lines above 120°C, although with reduced amplitudes. The amplitude of the drop in *c/a* as the temperature rises toward 120°C, and the sharpness of the discontinuity of the slope at 120°C seem to indicate the extent of the structural change and the ability to propagate tetragonal phonons. Notice in Fig. 5B that the *c/a* curves for BT10, BT50, and BT100 show very little indication of a structural change, and hence are expected to continue to display tetragonal Raman lines.

E. Structural coherence of the BTO nanoparticles

Figure 2A displays the PDFs of the five sizes of BTO nanoparticles examined with synchrotron high-energy X-rays. Often the decaying envelope of the PDF oscillations gives some sense of the structural coherence of the particles. Unfortunately in this case, the decay constants of the largest four particle sizes (Sakai particles) are indistinguishable from their respective reference materials, either LaB_6 or Ni, indicating their coherence decay lengths are indistinguishable from bulk material. We found a more promising indicator of the extent of structural coherence is provided by the decay of the fitted *c/a* ratio with increasing *r*-range as illustrated in Fig. 6B. In Section III we deduced from Fig. 6B a structural coherence length of somewhat less than 40 Å, i.e., a radius of eight or nine unit cells. What is the origin of this "decoherence" that reduces the effective tetragonality ($\equiv c/a - 1$) by an average of 25% for a fitting range of r = 1 to 60 Å? Random structural disorder is a cause that has been considered by several researchers,[11,15-17] but an ordered mesoscale-structure can also lead to a perceived loss of spatial correlation.

As an example of an ordered mesoscale-structure, Zhang et al.[29] have simulated bulk BTO using quantum mechanics and density functional theory and found an unusual structure which they have named the FE-AFE model (ferroelectric-antiferroelectric). Above 120°C the model becomes purely AFE in which Ti-O chains in all three directions contain Ti displacements of nearly alternating sign along body diagonals of the lattice unit cell. Each Ti-O chain carries a net polarization, but adjacent parallel Ti-O chains are arranged in such a way that the net polarization vanishes. This AFE model is a potential description of small BTO nanoparticles at RT through 120°C and above, though we have not found that it provides compellingly better fits to our PDFs than our standard tetragonal model.

As a second example, Fu and Bellaiche[31] use a first-principles-derived effective-Hamiltonian approach coupled with Monte Carlo simulations to calculate the structure of ~ 5 nm BTO particles. They find that the Ti displacements rotate from unit cell to unit cell, forming an unusual, complex "vortex-like" pattern. This pattern is influenced by the shape of the particle surface, and hence can be slightly less ordered than the AFE model above, but certainly the apparent spatial correlation length would be limited by these vortices of Ti displacements.

F. Summary

We have achieved a reasonably consistent picture of the structure of BTO nanoparticles (and of bulk BTO) by focusing on the values of *c/a* and Ti-displacement deduced from fits of X-ray PDFs acquired for a range of particle sizes and over a range of temperatures. An important point is that the fits to the PDFs were performed over different ranges of *r*: 1 to 20 Å for best insight into short-range structure, and 20 to 60 Å for a better grasp of long-range structure for comparison with XRD Bragg reflections. These short-range versus long range pictures have helped to reconcile apparently contradictory results from PDFs, Bragg reflections, and Raman spectra. The views from the two spatial scales have been key to detecting and documenting the phase transition experienced by the larger nanoparticles (equivalent to bulk) and the lack thereof in the smaller particles. And while these smaller, distinctively different BTO nanoparticles do *not* exhibit a sharp phase transition at 120°C, they already show long-range cubic order at RT that is gradually reinforced with increasing temperature. Ultimately, however, we fall short of a precise understanding of how random disorder or ordered mesoscale-structure (or both) facilitate a transition from short-range to long-range structure in which the *c/a* ratio is reduced but the Ti displacement is unaffected (or slightly increased).

ACKNOWLEDGMENTS

The authors wish to thank Dr. Susan Heidger of the Air Force Research Laboratory/High Power Microwave Electromagnetic Microwave Division for significant support of this work. Sandia National Laboratories is a multimission laboratory managed and operated by National Technology & Engineering Solutions of Sandia, LLC, a wholly owned subsidiary of Honeywell International Inc., for the U.S. Department of Energy's National Nuclear Security Administration under contract DE-NA0003525. PDF data collection and analysis by Shi and Billinge were supported by DOE Office of Science, Office of Basic Energy Sciences through contract DE-SC00112704. Use of the National Synchrotron Light Source, Brookhaven National Laboratory, was supported by DOE-BES under contract number DE-AC02-98CH10886. The authors also want to thank Jade Star Lackey and Jonathan Harris for use of the XRD lab and Charles Taylor for use of the Raman spectrometer in Pomona College's Geology and Chemistry Departments. We extend additional thanks to Caleah Whitten and Jonathan Miller for synthesizing the 10 nm BTO nanoparticles at Sandia Labs.

REFERENCES

* Author to whom correspondence should be addressed. Email: *tmonson@sandia.gov*

[1] Y. Ye, F. Dogan, E. Schamiloglu, and J. Gaudet, Proceedings of the 14th IEEE International Pulsed Power Conference, 2003, Institute of Electrical and Electronics Engineers 719 (2003).
[2] M. H. Frey, Z. Xu, P. Han, and D. A. Payne, Ferroelectrics **206-207**, 337 (1998).
[3] K. Uchino, *Ferroelectric Devices*, 2nd edition, Series Ed.: Vol. (CRC Press Taylor & Francis Group: Boca Raton, FL USA, 2010).
[4] G. Arlt, D. Hennings, and G. de With, J. Appl. Phys. **58**, 1619 (1985).
[5] G. H. Kwei, A. C. Lawson, S. J. L. Billinge, and S. W. Cheong, J. Phys. Chem. **97**, 2368 (1993).
[6] W. Cochran, Advances in Physics **9**, 387 (1960).
[7] I. B. Bersuker, Physics Letters **20**, 589 (1966).
[8] R. Comes, M. Lambert, and A. Guinier, Solid State Communications **6**, 715 (1968).
[9] P. R. Comes, M. Lambert, and A. Guinier, Acta Crystallographica **A26**, 244 (1970).
[10] G. H. Kwei, S. J. L. Billinge, S. W. Cheong, and J. G. Saxton, Ferroelectrics **164**, 57 (1995).
[11] K. Page, T. Proffen, M. Niederberger, and R. Seshadri, Chem. Mat. **22**, 4386 (2010).
[12] I. Levin, V. Krayzman, and J. C. Woicik, Physical Review B **89**, 024106-1 (2014).
[13] M. S. Senn, D. A. Keen, T. C. A. Lucas, J. A. Hriljac, and A. L. Goodwin, Physical Review Letters **116**, 207602-1 (2016).
[14] B. Ravel, E. A. Stern, R. I. Vedrinskii, and V. Kraizman, Ferroelectrics **206-207**, 407 (1998).
[15] V. Petkov, M. Gateshki, M. Niederberger, and Y. Ren, Chem. Mat. **18**, 814 (2006).
[16] M. B. Smith, K. Page, T. Siegrist, P. L. Redmond, E. C. Walter, R. Seshadri, L. E. Brus, and M. L. Steigerwald, J. Am. Chem. Soc. **130**, 6955 (2008).
[17] F. A. Rabuffetti, and R. L. Brutchey, J. Am. Chem. Soc. **134**, 9475 (2012).
[18] Y. Ikeda, M. Kuwai, S. Ogama, Y. Kuniyoshi, and K. Hidaka, US Patent 8431109 B2, Sakai Chemical Industry Co., Ltd., Osaka JP, April 30, 2013**,** *Process for Production of Composition.*
[19] S. Yoon, S. Baik, M. G. Kim, N. Shin, and I. Kim, J. Am. Ceram. Soc. **90**, 311 (2007).
[20] P. J. Chupas, X. Y. Qiu, J. C. Hanson, P. L. Lee, C. P. Grey, and S. J. L. Billinge, J. Appl. Crystallogr. **36**, 1342 (2003).
[21] A. P. Hammersley, S. O. Svensson, M. Hanfland, A. N. Fitch, and D. Hausermann, High Press. Res. **14**, 235 (1996).
[22] P. Juhas, T. Davis, C. L. Farrow, and S. J. L. Billinge, J. Appl. Crystallogr. **46**, 560 (2013).
[23] T. Egami, and S. J. L. Billinge, *Underneath the Bragg Peaks: Structural Analysis of Complex Materials*, 2nd edition, Series Ed.: R. W. Cahn, Pergamon Materials Series Vol. 7 (Elsevier Science: Oxford, UK, 2012).
[24] T. Proffen, and S. J. L. Billinge, J. Appl. Crystallogr. **32**, 572 (1999).
[25] C. L. Farrow, P. Juhas, J. W. Liu, D. Bryndin, E. S. Bozin, J. Bloch, T. Proffen, and S. J. L. Billinge, J. Phys.: Condens. Matter **19**, 335219 (2007).
[26] K. Page, T. Kolodiazhnyi, T. Proffen, A. K. Cheetham, and R. Seshadri, Phys. Rev. Lett. **101**, 205502 (2008).
[27] A. S. Masadeh, E. S. Bozin, C. L. Farrow, G. Paglia, P. Juhas, S. J. L. Billinge, A. Karkamkar, and M. G. Kanatzidis, Phys. Rev. B **76**, 115413 (2007).
[28] A. Scalabrin, A. S. Chaves, D. S. Shim, and S. P. S. Porto, Phys. Status Solidi B: Basic Research **79**, 731 (1977).
[29] Q. Zhang, T. Cagin, and W. A. Goddard, 3rd, Proc. Natl. Acad. Sci. USA **103**, 14695 (2006).
[30] TPL, Inc., *NanOxide™ HPB-1000 <100 nm Barium Titanate* **2005**, http://www.tplinc.com/uploads/HPB-1000_Technical_Bulletin.pdf, 08/02/2016.
[31] H. Fu, and L. Bellaiche, Phys. Rev. Lett. **91**, 257601 (2003).
[32] See Supplemental Material at [*URL will be inserted by publisher*] for additional XRD PDF data, XRD lab data, Raman spectra, and associated data analysis.

Table of Contents Graphic:

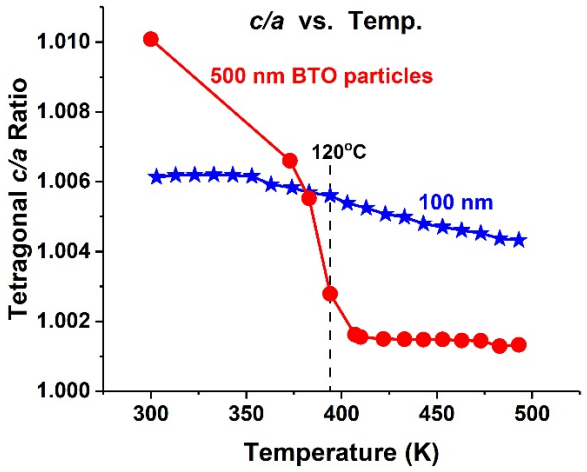

Aspect ratio: 11.4cm/9.00cm = 1.27